NANO LETTERS

pubs.acs.org/NanoLett

Letter

Deeply Rechargeable and Hydrogen-Evolution-Suppressing Zinc Anode in Alkaline Aqueous Electrolyte

Yamin Zhang, Yutong Wu, Wenqin You, Mengkun Tian, Po-Wei Huang, Yifan Zhang, Zhijian Sun, Yao Ma, Tianqi Hao, and Nian Liu*

Cite This: *Nano Lett.* 2020, 20, 4700–4707

Read Online

ACCESS | Metrics & More | Article Recommendations | Supporting Information

ABSTRACT: Metallic zinc as a rechargeable anode material for aqueous batteries has gained tremendous attention. Zn-air batteries, which operate in alkaline electrolytes, are promising with the highest theoretical volumetric energy density. However, rechargeable zinc anodes develop slowly in alkaline electrolytes due to passivation, dissolution, and hydrogen evolution issues. In this study, we report the design of a submicron zinc anode sealed with an ion-sieving coating that suppresses hydrogen evolution reaction. The design is demonstrated with ZnO nanorods coated by TiO_2, which overcomes passivation, dissolution, and hydrogen evolution issues simultaneously. It achieves superior reversible deep cycling performance with a high discharge capacity of 616 mAh/g and Coulombic efficiency of 93.5% when cycled with 100% depth of discharge at lean electrolyte. It can also deeply cycle ~350 times in a beaker cell. The design principle of this work may potentially be applied to other battery electrode materials.

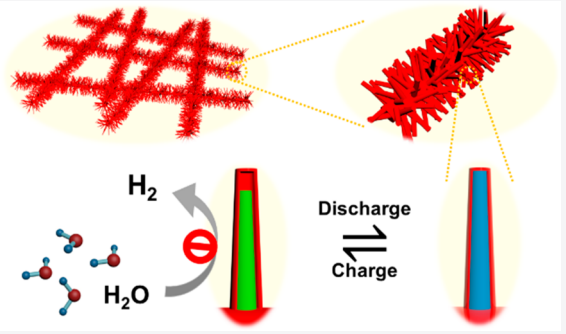

KEYWORDS: *Zinc, aqueous electrolyte, battery, hydrogen evolution*

INTRODUCTION

Lithium-ion batteries (LIBs) have achieved great success due to their high energy density and high rechargeability.[1−3] However, the increasing concerns about safety, cost, and limited critical raw materials motivate the exploration of alternative battery systems.[4,5] Besides, safety is more difficult to manage with the increasing scale of the battery unit. Compared with flammable organic electrolytes, batteries with aqueous electrolytes generally feature better intrinsic safety, higher ionic conductivity, and lower cost.[6−11] Among metals that are stable in water, zinc has the lowest redox potential (−0.762 V versus standard hydrogen electrode) and thus is the most active metal anode compatible with aqueous electrolytes. Moreover, zinc possesses high theoretical capacity (820 mAh g^{-1}), high volumetric capacity (5854 mAh cm^{-3}), low cost, and low toxicity, which make it particularly advantageous.[12−14] These distinctive merits as well as new technologies codeveloped with LIBs, such as precise electrode material synthesis,[15] advanced accessory cell components,[16] and powerful diagnosis techniques,[17,18] have prepared a potential revival of zinc-based aqueous batteries.[19] Pairing zinc anodes with oxygen cathodes can yield Zn-air batteries,[20,21] which have prominent theoretical gravimetric and volumetric energy densities (1093 Wh/kg, 6134 Wh/L). Although primary Zn-air batteries have been available in the market for long-duration, low-rate applications, deeply rechargeable ones have not been commercially successful. Also, the practical energy densities of Zn-air batteries are usually between 350 and 500 Wh/kg.[22] Further rational design and engineering of both cathode and anode materials are required to achieve high energy-density Zn-air batteries.

Neutral and alkaline electrolytes are two major classes of aqueous electrolytes for zinc anodes. Research on rechargeable zinc anodes in neutral electrolytes[13,23] has achieved great progress in the past decade; examples include the discoveries of "water-in-salt" electrolytes[12] and molten hydrate electrolytes.[24] Nonetheless, cycling zinc anodes deeply in alkaline electrolytes remains challenging due to the dramatic change of the chemical and physical forms of zinc species and the severe hydrogen evolution side reaction during cycling.[25] Despite the challenges, it is vital to enable highly rechargeable zinc anodes in alkaline electrolytes to propel the development of rechargeable Zn-air batteries, as air cathodes kinetically favor alkaline electrolytes over neutral ones.[26,27] Even though nonalkaline electrolytes were previously investigated for Zn−air batteries,[28] their ORR and OER kinetics at the air cathode are slow. Thus, it is still necessary to study alkaline electrolytes.

Received: April 23, 2020
Revised: May 23, 2020
Published: May 26, 2020

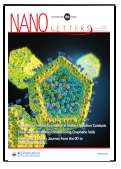

https://dx.doi.org/10.1021/acs.nanolett.0c01776
Nano Lett. 2020, 20, 4700−4707

In alkaline electrolytes, there are two consecutive zinc conversion reactions (eqs 1 and 2). This solid-solute-solid mechanism inherently causes passivation and dissolution issues on zinc anodes. These issues are due to the following processes: (i) the insulating discharge product ZnO passivates the surface of zinc anodes, preventing the latter from further discharging or recharging back to metallic zinc (Figure 1a),

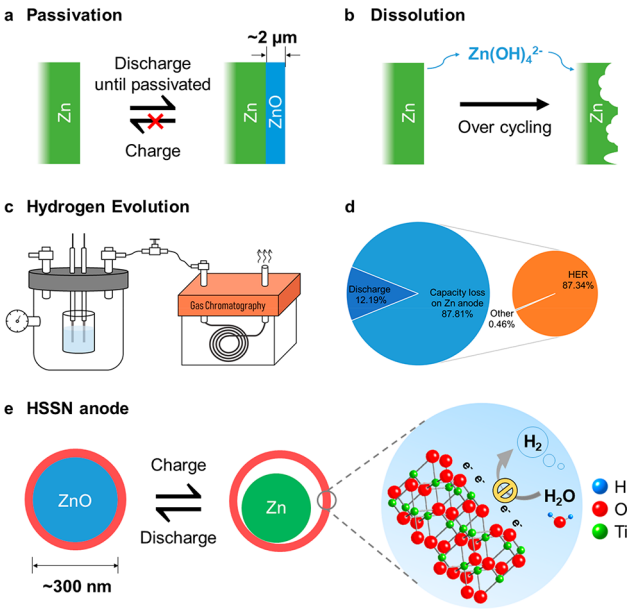

Figure 1. Typical issues of Zn anodes in alkaline electrolyte and design of a high-performance Zn anode by overcoming the issues. (a, b) Schematic diagrams of (a) passivation and (b) dissolution issues of zinc anodes. (c) Schematic diagram of the battery-GC quantitative analysis method to quantitatively identify the influence of HER on Coulombic efficiency of zinc anodes by measuring the H_2 evolved in the reactor after charging/discharging the zinc anode for 1 cycle. (d) Distribution of the charged capacity on the zinc anode in a Zn−Ni battery. The capacity loss on the Zn anode is almost fully caused by HER. Thus, HER suppressing zinc anodes should possess high Coulombic efficiency. (e) Schematic illustration of the zinc anode design principle: sealed submicron-sized anodes with a HER suppressing ion-sieving coating to overcome passivation, dissolution, and hydrogen evolution issues simultaneously in alkaline electrolytes.

and (ii) the intermediate zincate ($Zn(OH)_4^{2-}$) is soluble in alkaline electrolytes, which leads to active material loss, random ZnO precipitation on the electrode, and morphology change of the electrode over cycling (Figure 1b). In addition, the hydrogen evolution reaction (HER, eq 3) is a side reaction on the zinc anode. In an alkaline electrolyte with pH 14, the Zn/ZnO standard reduction potential (−1.26 V vs standard hydrogen electrode (SHE)) is lower than that of the HER (−0.83 V vs SHE). Thus, HER is thermodynamically favored during charging, which causes low Coulombic efficiency, electrolyte drying, bubble accumulation, and eventually cell failure. We have created a battery-gas chromatography (GC) quantitative analysis method (Figures 1c and S1) to identify the influence of HER on the capacity loss of zinc anodes. This is achieved by measuring the evolved H_2 using GC after charging/discharging the zinc anode in alkaline electrolyte (ZnO-saturated 4 M KOH) for one cycle (Figure S2), as discussed in the Materials and Methods. The cathode and overall reactions can be found in eqs 4 and 5. It is worth noting that the amount of NiOOH was in excess, which could guarantee the full depletion of Zn in the discharge step. In other words, the capacity loss (charge capacity-discharge capacity) on Zn anodes is attributed to side reactions on Zn anodes. As shown in Figure 1d, the capacity loss on the Zn anode is almost fully caused by HER (99.47% = 87.34%/87.81%). The other 0.46% of capacity loss might be caused by the oxidation of Zn[29] through reacting with O_2. In consideration of Zn anodes, HER suppressing Zn anodes should possess high Coulombic efficiency (discharge capacity/charge capacity).

$$\text{Complexation: } ZnO + H_2O + 2OH^- \leftrightarrow Zn(OH)_4^{2-} \quad (1)$$

$$\text{Anode: } Zn(OH)_4^{2-} + 2e^- \leftrightarrow Zn + 4OH^- \quad (2)$$

$$\text{HER: } 2H_2O + 2e^- \rightarrow H_2 + 2OH^- \quad (3)$$

$$\text{Cathode: } 2NiOOH + 2H_2O + 2e^- \leftrightarrow 2Ni(OH)_2 + 2OH^- \quad (4)$$

$$\text{Overall: } 2NiOOH + Zn + H_2O \leftrightarrow 2Ni(OH)_2 + Zn \quad (5)$$

Attempts have been made in the past to overcome one or two of passivation, dissolution, and HER issues. For example, submicron-sized structures,[30,31] composites with highly conductive materials,[32−34] and 3D high surface area electrodes[35,36] have been shown to be effective in addressing the ZnO passivation issue. Surface protective coatings[37−39] have been demonstrated to slow down the loss of zinc active material. Surface treatments[40,41] and additives[42] have been used to suppress the HER. However, there are very few successful examples that address these issues simultaneously.

In this work, we seal submicron-sized anodes by coating them with a HER suppressing ion-sieving layer to tackle simultaneously passivation, dissolution, and HER issues (Figure 1e). Our design features the following advantages: (i) submicron-sized ZnO avoids passivation and allows complete utilization of the active materials; (ii) ion-sieving coating layer confines zincate inside and mitigates shape changes of the electrode; and (iii) the coating layer is made of HER suppressing material, which represses side reactions. Our results demonstrate that HER suppressing sealed nanorod (HSSN) zinc anodes exhibit long cycle life, high Coulombic efficiency, and high specific discharge capacity.

RESULTS AND DISCUSSION

The critical thickness of ZnO passivation layer has previously been quantified to be ~2 μm when a zinc metal anode is completely passivated.[37] Thus, submicron-sized zinc anodes are believed to be able to overcome the passivation problem. However, decreasing the feature size to be nanoscale will intensify the dissolution and HER problems due to increased electrode−electrolyte contact area.[43] Therefore, we propose to seal submicron-sized anodes by uniformly coating a HER suppressing ion-sieving layer, which can suppress HER and selectively block larger zincate ions inside the coating while enabling OH^-/H_2O transport (Figure 1e). Some Zn anodes have been reported to have the above-proposed structure, such as Al_2O_3 coated Zn powders,[40] $Li_2O-2B_2O_3$ coated Zn powders,[41] and TiO_2−Coated ZnO.[44] However, there is a lack of evidence showing that the coating is uniform, with either no or unclear TEM images. As a result, these structures may still suffer dissolution and HER issues, which might be the

https://dx.doi.org/10.1021/acs.nanolett.0c01776
Nano Lett. 2020, 20, 4700−4707

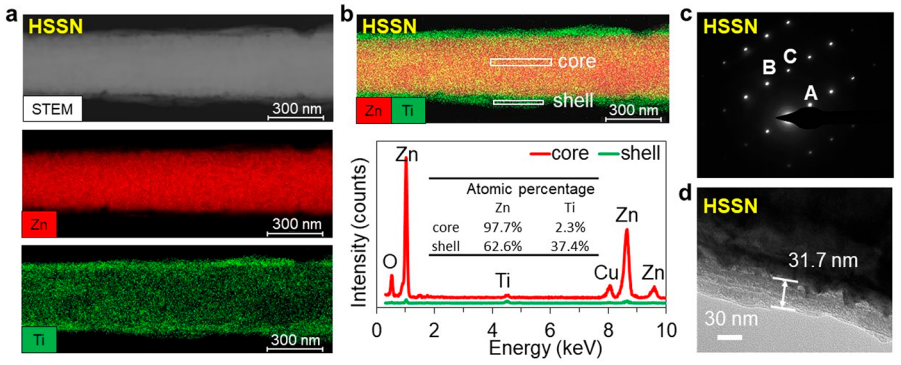

Figure 2. Characterization of a single ZnO@TiO_2 nanorod collected from the HSSN anode. (a) STEM image and elemental mappings of a ZnO@TiO_2 nanorod. (b) Spatial distributions of Zn and Ti elements and EDX spectroscopies in the core and shell regions. (c) Transmission electron microscopy (TEM) diffraction image of a ZnO@TiO_2 nanorod, showing diffraction pattern of hexagonal ZnO. A [002]; B [110]; C [112]. (d) TEM image of a ZnO@TiO_2 nanorod, showing the thickness (~30 nm) of TiO_2 coating.

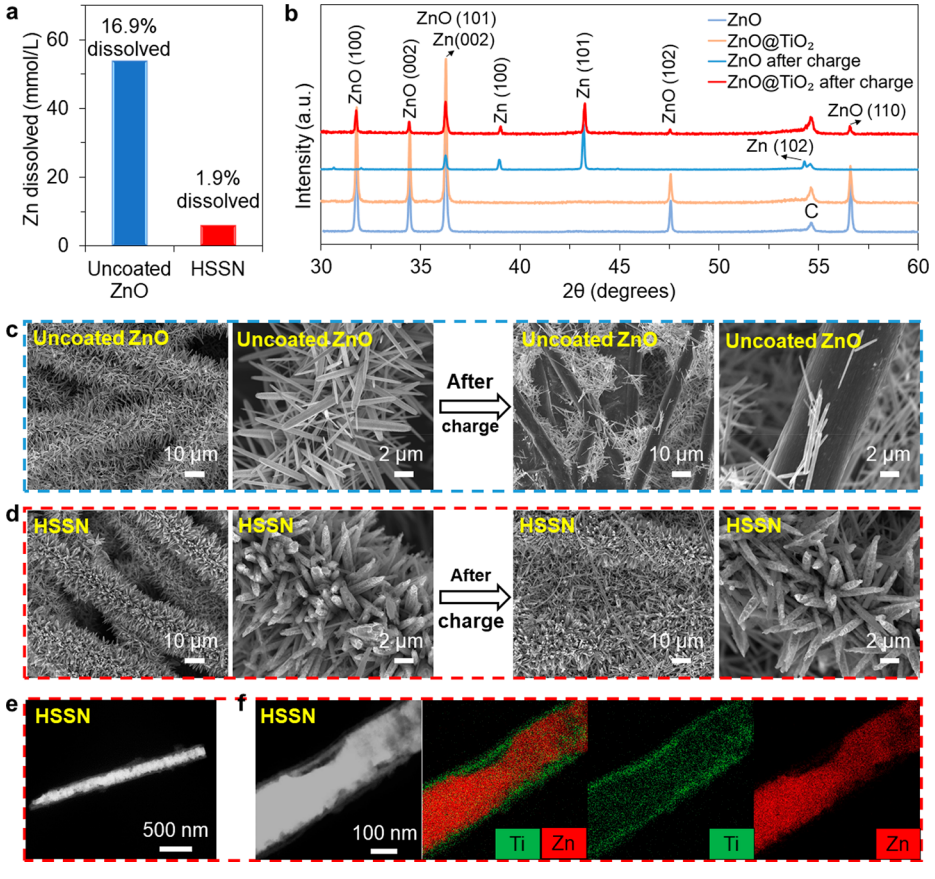

Figure 3. Characterization of zinc anodes before and after charging. (a) ICP results showing dissolved Zn concentration after soaking the HSSN and the uncoated ZnO anodes in 4 M KOH solution. And 90% ZnO dissolution is suppressed in the HSSN anode, which means that the TiO_2 coating effectively blocks zincate ions. (b) XRD patterns of the uncoated ZnO and the HSSN anodes before and after charging. The weak ZnO peaks of the HSSN anode after charging are from residual unreacted ZnO. (c, d) SEM images before and after charging (c) the uncoated ZnO anode and (d) the HSSN anode. (e) STEM image of a ZnO@TiO_2 nanorod after charging. (f) STEM image and elemental mappings of a ZnO@TiO_2 nanorod after charging. The same anode sample was used to obtain panels d–f.

reason for their short cycle life (<20 cycles)[40,41] and low specific discharge capacity.[44] We have also reported a ZnO@TiN_xO_y anode,[39] which could address the dissolution issue while the HER issue still exists. In this study, we chose TiO_2 as the coating material here to demonstrate our concept, as it is stable with alkaline electrolytes and has been reported to have low HER activity.[45] A binder-free self-supporting ZnO nanorod anode was chosen as the model system for this study because its structure and morphology can be easily studied. This design principle is applicable to Zn anodes with other structures and coating materials.

The HSSN anode was successfully fabricated as shown in Figure S3. ZnO nanorods were first grown on the carbon paper hydrothermally.[46] The mass loading of ZnO nanorods on carbon paper can be tuned from 0.5 mg/cm^2 to 5.5 mg/cm^2 (Table S1 and Figure S4). The TiO_2 layer was coated on the

https://dx.doi.org/10.1021/acs.nanolett.0c01776
Nano Lett. 2020, 20, 4700–4707

ZnO nanorods via a mild solution method at room temperature.[47] The ZnO nanorods were immersed in an aqueous solution consisting of 0.075 M $(NH_4)_2TiF_6$ and 0.2 M H_3BO_3. After the TiO_2 coating, the ZnO nanorod structure was well maintained (Figure S5). Scanning transmission electron microscopy (STEM) image and elemental mappings (Figure 2a) of the HSSN anode confirm that the TiO_2 coating is uniform. We also obtained spatial distributions of Zn and Ti by taking energy-dispersive X-ray (EDX) spectroscopies in the core and shell regions (Figure 2b). The core region shows a much higher Zn intensity than that of the shell region, which further affirms the ZnO core/TiO_2 shell structure. During synthesis, $(NH_4)_2TiF_6$ hydrolyzed to TiO_2 on the surface of ZnO, while surface ZnO slightly dissolved in the solution with acids produced by $(NH_4)_2TiF_6$ hydrolysis.[47] Thus, we believe that some Zn species went into the TiO_2 coating during the synthesis, which may explain the Zn signal on the TiO_2 shell. As evidenced by Figure 2c, the ZnO in the core has a hexagonal close packed crystal structure, and the TiO_2 coating is amorphous. The TiO_2 layer has a thickness of ~31.7 nm (Figure 2d). The mass loading of TiO_2 is ~0.35 mg/cm^2, which is only ~10.4 wt % of the HSSN anode (with 3 mg/cm^2 ZnO nanorods). After the ZnO was etched away, the hollow nanoarrays stayed in place (Figure S6), displaying that the TiO_2 coating, although only 30 nm thick, is mechanically strong and firmly supports the ZnO nanorods.

To evaluate the capability of the TiO_2 shell to suppress zincate dissolution, we soaked both the HSSN and the uncoated ZnO anodes in ZnO-free 4 M KOH solution for 15 min. The ratio of ZnO active material mass and solution volume was 0.02 mg/μL. We then measured the dissolved Zn concentration in both solutions using inductively coupled plasma atomic emission spectroscopy (ICP-AES). As shown in Figure 3a, the dissolved Zn of the HSSN anode (1.9%) is much lower than that of the uncoated ZnO anode (16.9%). And 90% ZnO dissolution is suppressed in the HSSN anode, which displays that the TiO_2 shell effectively blocks zincate ions. We imaged both anodes after soaking in 4 M KOH solution (Figure S7), which also supports that TiO_2 coating can effectively confine zincates inside the shell.

The zinc-based anodes were also characterized before and after a single charge in coin cells. As shown in Figure 3b, XRD patterns confirmed the existence of the charging product, metallic Zn. After being charged at 0.25 mA/cm^2 for 1.5 h, the uncoated ZnO nanorod anode showed severe structural degradation. The nanorods detach from carbon paper (Figure 3c). In contrast, the HSSN anode has no obvious shape change (Figure 3d). Additionally, the HSSN anode kept nearly unchanged after five cycles (Figure S8). STEM images and elemental mappings of the HSSN anode after charging are presented in Figures 3e,f and S9. These results indicate that the TiO_2 shell confines zinc active materials inside during cycling, which can be attributed to the ion-sieving effect of the TiO_2 shell. As shown in the N_2 absorption spectrum (Figure S10), TiO_2 layer has nanosized pores, which block larger zincate ions inside the shell and enable OH^-/H_2O transport through the shell. Further explanation for the ion-sieving effect of the shell can be found in our previous study.[37] The porosity of TiO_2 can potentially be further engineered to optimize its ion-sieving performance.

As discussed above, an ion-sieving coating layer is necessary for nanostructured Zn anodes to suppress active material dissolution. In consideration of HER, such an ion-sieving coating layer should be HER suppressing. To evaluate the HER suppressing capability of the TiO_2 shell and its effect on the Coulombic efficiency, we investigated HER activities of TiO_2 and TiN_xO_y. TiN_xO_y (Figure S11) was chosen to be the control material because its uniform coating and ion-sieving property have been achieved.[39] To best represent our anodes, we etched ZnO away from HSSN and ZnO@TiN_xO_y anodes to get TiO_2 and TiN_xO_y hollow nanorod coatings on carbon paper substrates, respectively (Figure S12). We then assembled three-electrode cells in 4 M KOH electrolyte with TiO_2 or TiN_xO_y electrode as the working electrode, Hg/HgO electrode as the reference electrode, and Pt foil as the counter electrode (Figures S13 and S14). As shown in IR-corrected polarization curves (Figure 4a), the HER on the TiN_xO_y electrode was

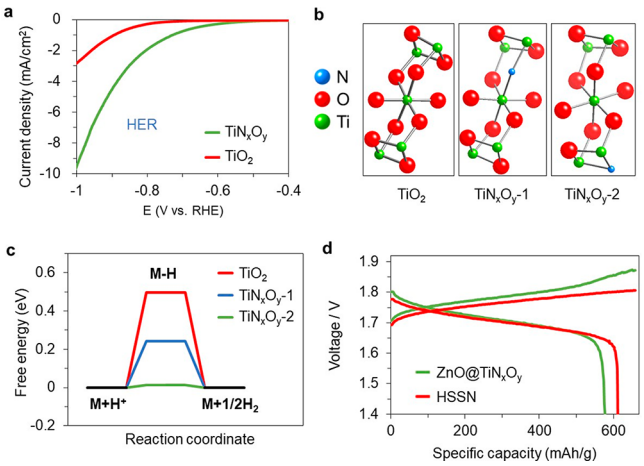

Figure 4. Hydrogen suppressing property of TiO_2. (a) IR-corrected polarization curves of TiN_xO_y and TiO_2 electrodes. At any fixed potential, the hydrogen evolution on the TiN_xO_y electrode is severer than the TiO_2 electrode. Scan rate: 2 mV/s. (b) Basic models and (c) adsorption free energy diagram of TiO_2, TiN_xO_y-1, and TiN_xO_y-2 clusters. (d) Voltage profiles of Zn−Ni batteries with HSSN and ZnO@TiN_xO_y as anodes. The Coulombic efficiency of the HSSN anode is higher with better HER suppressing capability.

more severe (higher current density at a fixed HER potential) than on TiO_2. These experimental results reveal that the TiO_2 is more hydrogen suppressive than TiN_xO_y. In addition, we also compared the HER activities of the TiO_2 electrode with the carbon paper substrate, which experimentally indicates that the existence of TiO_2 coating can suppress HER (Figure S15). To understand the hydrogen suppressing property of TiO_2, we have measured the sheet resistance of TiO_2 and TiN_xO_y using a four-point probe system (Figure S16). TiO_2 has lower electrical conductivity, which may be part of the reason for its lower HER activity and better HER suppressing capability. Simulations based on the force field model were also conducted to confirm the hydrogen suppressing property of TiO_2. Cluster rather than slab model was chosen because of its applicability in representing amorphous materials (Figure 4b).[48] In a three-state diagram (Figure 4c), ΔG_H^* represents the free energy for H adsorption. The material with higher $|\Delta G_H^*|$ value possesses lower catalytic activity[49,50] and better hydrogen suppressing capability. The free energy for TiO_2 is 0.495 eV, which is higher than that of TiN_xO_y clusters (Figure S17 and Table S2). This result illustrates that TiO_2 is the most hydrogen suppressive.

https://dx.doi.org/10.1021/acs.nanolett.0c01776
Nano Lett. 2020, 20, 4700−4707

As shown in Figures S18 and S19, HSSN and ZnO@TiN$_x$O$_y$ anodes have very similar ion-sieving capabilities. With hydrogen suppressing capability, the HSSN anode shows higher Coulombic efficiency compared to the ZnO@TiN$_x$O$_y$ counterpart. To specifically focus on Zn anodes, for all the cells shown below, cathodes with excess capacity were harvested to pair with Zn anodes. The calculation of the specific capacity of zinc anodes is based on the mass of ZnO (theoretical capacity: 658 mAh/g) if not otherwise specified. Cells were galvanostatically cycled at a charge rate of 1C and a discharge rate of 5C.[51] We cycled our anodes in pouch cells (Figure S20) instead of coin cells to avoid the HER on stainless steel coin cell cases.[52] They were cycled at 100% depth of discharge (DOD). Thus, the extent of side reactions on them can be directly indicated by the cell Coulombic efficiency. Higher "clean" Coulombic efficiency means fewer side reactions. The charge/discharge profiles of HSSN and ZnO@TiN$_x$O$_y$ anodes cycled in lean electrolyte (100 μL) are plotted in Figure 4d. Their cycling performance and rate-capability tests can be found in Figures S21 and S22. The average Coulombic efficiency (93.50%) of the HSSN anode in the first 12 galvanostatic cycles is much higher than that of the ZnO@TiN$_x$O$_y$ anode (84.96%). Even though TiO$_2$ has lower electrical conductivity than TiN$_x$O$_y$, the HSSN anode showed slightly better rate capability than the ZnO@TiN$_x$O$_y$ anode, which may be because there are more pores on the HSSN anode, and thus, the faster OH$^-$/H$_2$O transport can be achieved through the TiO$_2$ shell (Figure S23). The HSSN anode achieves higher Coulombic efficiency of 93.09% than the ZnO@TiN$_x$O$_y$ anode (88.07%). In similar alkaline electrolytes with 100% DOD, most previous reports show Coulombic efficiency lower than 90% (Table S3).

As shown in Figures 5a and S24, when cycled at 40% DOD in lean electrolyte, the HSSN anode (with 1.05 mg/cm^2 ZnO)

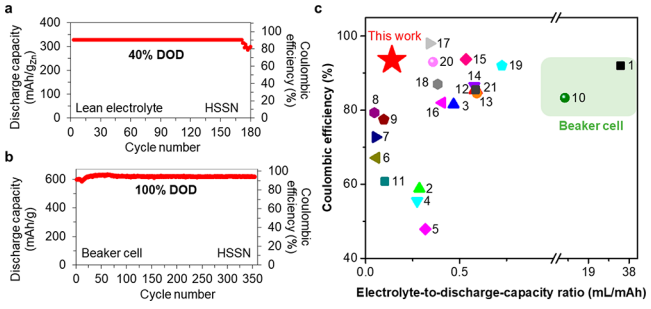

Figure 5. Electrochemical performance of HSSN anodes. (a) Cycling performance of the HSSN anode in lean electrolyte at 40% DOD. (b) Cycling performance of the HSSN anode in a beaker cell with a large amount of electrolyte at 100% DOD. (c) Comparison of our HSSN anode and previously reported anodes (with 100% DOD) in aspects of E/DC ratio and Coulombic efficiency.

demonstrated long-term stable cycling for more than 170 cycles. We confirmed that there was no capacity contribution from the TiO$_2$ shell during the electrochemical reactions (Figure S25). When cycled at 100% DOD in lean electrolyte, the HSSN anode (with 1.5 mg/cm^2 ZnO) achieved an average Coulombic efficiency of 93.5% and average discharge capacity of 616 mAh/g in the first 12 galvanostatic cycles (Figure S21). The capacity fading occurs after 33 cycles. The battery failure can be attributed to (1) the structural collapse of the HSSN anode (Figure S26) due to the shape and volume changes of Zn/ZnO inside the shell and (2) the limited mass transfer of Zn species caused by electrolyte decomposition and hydrogen accumulation. We also evaluated our anode in a beaker cell with a large amount of ZnO-saturated electrolyte. As shown in Figure 5b, the HSSN anode (with 1.6 mg/cm^2 ZnO) was cycled more than 350 times with Coulombic efficiency of 94.3% and a discharge capacity of 621 mAh/g. Voltage profiles for the batteries shown in Figure 5a and b can be found in Figure S27. From the above cycling results, we can conclude that the cycle life of Zn anodes in lean electrolyte is much shorter than in a large amount of ZnO-saturated electrolyte. This can be explained by the electrochemistry of alkaline Zn anodes. In a large amount of ZnO-saturated electrolyte, the effect of minor electrolyte decomposition can be minimized with excess water. Moreover, there is excess zincate in the electrolyte, which is the active material for Zn anodes. With a large capacity contribution from the zincate supplied from the electrolyte, the long cycle life of Zn anodes can be achieved, yet it is inauthentic. In lean electrolyte (100 μL), batteries fail quicker as a result of complicated synergistic effects caused by electrolyte decomposition and limited mass transfer of Zn species. However, it is still necessary to cycle anodes in lean electrolyte to evaluate their true performance, which can represent practical situations despite their short cycle life.

Electrolyte-to-discharge-capacity (E/DC) ratio is also critical for device-level energy density and is crucial for practical applications. It has been paid attention in lithium-based nonaqueous batteries.[53−55] Recently, researchers in the zinc-based battery field have begun emphasizing the low E/DC ratio.[56,57] The tested Coulombic efficiency of alkaline Zn anodes is highly correlated to the E/DC ratio. Thus, it is necessary to provide E/DC ratios to get a fair comparison on the Coulombic efficiency of different Zn anode materials. However, only a few previous works (summarized in Table S4) reported this ratio or provided necessary information for its calculation. Here, we summarized them and compared our anode with them in terms of Coulombic efficiency and E/DC ratio in Figure 5c. Notably, to get a comparison on "clean" Coulombic efficiency of different Zn anodes, only deeply cycled Zn anodes with 100% DOD are listed above. Partially utilized (DOD < 100%) metallic zinc anodes are not included in the comparison because their Coulombic efficiencies cannot indicate the extent of side reactions occurring on Zn anodes. In comparison, our anode achieves a superior Coulombic efficiency (93.5%) at a low E/DC ratio (0.14 mL/mAh), which suggests the advance of our designed functionally coated Zn anodes (Figure S21). With the featured HER suppressing core/shell Zn anode, (1) Zn species are confined inside the shell so there is minimized active material loss, and (2) minimized HER and less electrolyte decomposition can be achieved with the HER suppressing property. These enable our anode to achieve high Coulombic efficiency in lean electrolyte. The overall areal and specific discharge capacities of the HSSN anode were ∼0.9 mAh/cm^2 and ∼91 mAh/g, respectively, after considering the mass of the current collector. Because of its specially featured core/shell nanorod structure, its overall capacity is unable to meet the requirement for practical Zn anodes (11.7 mAh/cm^2).[57] However, the design principal presented here may help guide further research to achieve practically high energy-density Zn anodes.

CONCLUSION

In summary, we have reported a zinc anode design, namely sealing submicron-sized ZnO with a HER suppressing and ion-

https://dx.doi.org/10.1021/acs.nanolett.0c01776
Nano Lett. 2020, 20, 4700−4707

sieving layer, to overcome simultaneously passivation, dissolution, and hydrogen evolution issues in alkaline electrolytes. A ZnO nanorod anode and TiO_2 shell were chosen to demonstrate this concept. The fabricated HSSN anode achieves superior reversible deep cycling performance at lean electrolyte. While the Coulombic efficiency of the HSSN anode is higher than that of most of the previously reported zinc anodes, it needs to be further improved to approach the efficiency of LIBs (99.9%). Optimization of the shell material, from aspects of pore size, porosity, and surface charge, may lead to further improvement of anode performance and stability. Other materials with controlled ion-sieving and HER suppressing properties also have the potential to be applied as the shell material. This design principle can potentially be applied to other morphologies (e.g., particles) of starting materials for large scale production. The mechanistic understanding and design principle reported in this study may also guide future design of other rechargeable high-energy aqueous batteries.

■ ASSOCIATED CONTENT

Supporting Information

The Supporting Information is available free of charge at https://pubs.acs.org/doi/10.1021/acs.nanolett.0c01776.

Experimental method, simulation, summary and comparison of E/DC ratio and Coulombic efficiency, additional characterization results on electrodes (PDF)

■ AUTHOR INFORMATION

Corresponding Author

Nian Liu − *School of Chemical and Biomolecular Engineering, Georgia Institute of Technology, Atlanta, Georgia 30332, United States;* orcid.org/0000-0002-5966-0244; Email: nian.liu@chbe.gatech.edu

Authors

Yamin Zhang − *School of Chemical and Biomolecular Engineering, Georgia Institute of Technology, Atlanta, Georgia 30332, United States;* orcid.org/0000-0003-4890-1265

Yutong Wu − *School of Chemical and Biomolecular Engineering, Georgia Institute of Technology, Atlanta, Georgia 30332, United States;* orcid.org/0000-0003-1214-9147

Wenqin You − *School of Chemical and Biomolecular Engineering, Georgia Institute of Technology, Atlanta, Georgia 30332, United States*

Mengkun Tian − *The Institute for Electronics and Nanotechnology, Georgia Institute of Technology, Atlanta, Georgia 30332, United States;* orcid.org/0000-0003-2790-7799

Po-Wei Huang − *School of Chemical and Biomolecular Engineering, Georgia Institute of Technology, Atlanta, Georgia 30332, United States*

Yifan Zhang − *School of Chemistry & Biochemistry, Georgia Institute of Technology, Atlanta, Georgia 30332, United States*

Zhijian Sun − *School of Materials Science and Engineering, Georgia Institute of Technology, Atlanta, Georgia 30332, United States*

Yao Ma − *School of Chemical and Biomolecular Engineering, Georgia Institute of Technology, Atlanta, Georgia 30332, United States;* orcid.org/0000-0002-8283-8645

Tianqi Hao − *School of Chemical and Biomolecular Engineering, Georgia Institute of Technology, Atlanta, Georgia 30332, United States*

Complete contact information is available at: https://pubs.acs.org/10.1021/acs.nanolett.0c01776

Author Contributions

Y.Z. and N.L. conceived the idea and cowrote the manuscript. Y.Z. carried out the synthesis, material characterization, and electrochemical measurements. Y.W. conducted the ALD. Y.Z. and W.Y. conducted the simulation. M.T., P.H., Y.Z., Z.S., Y.M., and T.H. assisted with material characterization and electrochemical measurements. All authors discussed the results and commented on the manuscript.

Notes

The authors declare no competing financial interest.

■ ACKNOWLEDGMENTS

N.L. acknowledges support from faculty startup funds from the Georgia Institute of Technology. The authors thank Prof. David S. Sholl for the useful discussion. Prof. Sankar Nair is acknowledged for allowing access to some laboratory apparatus. The authors thank Chris Yang, Yimeng Lyu, Peng Chen, Haochen Yang, Tzu-Ho Wu, and Anmol Mathur for assistance in experiments. The reactor for GC analysis was made by the Machine Research Services group in the School of Chemical & Biomolecular Engineering at Georgia Institute of Technology. Material characterization was performed in part at the Georgia Tech Institute for Electronics and Nanotechnology, a member of the National Nanotechnology Coordinated Infrastructure, which is supported by the National Science Foundation (Grant No. ECCS-1542174).

■ REFERENCES

(1) Chu, S.; Cui, Y.; Liu, N. The Path towards Sustainable Energy. *Nat. Mater.* **2017**, *16* (1), 16−22.

(2) Goodenough, J. B.; Park, K. The Li-Ion Rechargeable Battery: A Perspective. *J. Am. Chem. Soc.* **2013**, *135* (4), 1167−1176.

(3) Zhang, Y.; Liu, N. Nanostructured Electrode Materials for High-Energy Rechargeable Li, Na and Zn Batteries. *Chem. Mater.* **2017**, *29* (22), 9589−9604.

(4) Kim, H.; Hong, J.; Park, K. Y.; Kim, H.; Kim, S. W.; Kang, K. Aqueous Rechargeable Li and Na Ion Batteries. *Chem. Rev.* **2014**, *114* (23), 11788−11827.

(5) Lin, K.; Chen, Q.; Gerhardt, M. R.; Tong, L.; Kim, S. B.; Eisenach, L.; Valle, A. W.; Hardee, D.; Gordon, R. G.; Aziz, M. J.; et al. Alkaline Quinone Flow Battery. *Science* **2015**, *349* (6255), 1529−1532.

(6) Liang, Y.; Jing, Y.; Gheytani, S.; Lee, K. Y.; Liu, P.; Facchetti, A.; Yao, Y. Universal Quinone Electrodes for Long Cycle Life Aqueous Rechargeable Batteries. *Nat. Mater.* **2017**, *16* (8), 841−848.

(7) Luo, J.-Y.; Cui, W.-J.; He, P.; Xia, Y.-Y. Raising the Cycling Stability of Aqueous Lithium-Ion Batteries by Eliminating Oxygen in the Electrolyte. *Nat. Chem.* **2010**, *2* (9), 760−765.

(8) Bin, D.; Liu, Y.; Yang, B.; Huang, J.; Dong, X.; Zhang, X.; Wang, Y.; Xia, Y. Engineering a High-Energy-Density and Long Lifespan Aqueous Zinc Battery via Ammonium Vanadium Bronze. *ACS Appl. Mater. Interfaces* **2019**, *11* (23), 20796−20803.

(9) Xie, J.; Zhang, Q. Recent Progress in Multivalent Metal (Mg, Zn, Ca, and Al) and Metal-Ion Rechargeable Batteries with Organic Materials as Promising Electrodes. *Small* **2019**, *1805061*, 1805061.

(10) Park, M.; Beh, E. S.; Fell, E. M.; Jing, Y.; Kerr, E. F.; De Porcellinis, D.; Goulet, M.-A.; Ryu, J.; Wong, A. A.; Gordon, R. G.; et al. A High Voltage Aqueous Zinc−Organic Hybrid Flow Battery. *Adv. Energy Mater.* **2019**, *9* (25), 1900694.

(11) Wang, X.; Liao, Z.; Fu, Y.; Neumann, C.; Turchanin, A.; Nam, G.; Zschech, E.; Cho, J.; Zhang, J.; Feng, X. Confined Growth of Porous Nitrogen-Doped Cobalt Oxide Nanoarrays as Bifunctional Oxygen Electrocatalysts for Rechargeable Zinc−Air Batteries. *Energy Storage Mater.* **2020**, *26*, 157−164.
(12) Wang, F.; Borodin, O.; Gao, T.; Fan, X.; Sun, W.; Han, F.; Faraone, A.; Dura, J. A.; Xu, K.; Wang, C. Highly Reversible Zinc Metal Anode for Aqueous Batteries. *Nat. Mater.* **2018**, *17* (6), 543−549.
(13) Zhang, N.; Cheng, F.; Liu, J.; Wang, L.; Long, X.; Liu, X.; Li, F.; Chen, J. Rechargeable Aqueous Zinc-Manganese Dioxide Batteries with High Energy and Power Densities. *Nat. Commun.* **2017**, *8* (1), 405.
(14) Wu, T.-H.; Zhang, Y.; Althouse, Z. D.; Liu, N. Nanoscale Design of Zinc Anodes for High-Energy Aqueous Rechargeable Batteries. *Mater. Today Nano* **2019**, *6*, 100032.
(15) Ma, J.; Sung, J.; Hong, J.; Chae, S.; Kim, N.; Choi, S.-H.; Nam, G.; Son, Y.; Kim, S. Y.; Ko, M.; et al. Towards Maximized Volumetric Capacity via Pore-Coordinated Design for Large-Volume-Change Lithium-Ion Battery Anodes. *Nat. Commun.* **2019**, *10* (1), 475.
(16) Liu, K.; Liu, W.; Qiu, Y.; Kong, B.; Sun, Y.; Chen, Z.; Zhuo, D.; Lin, D.; Cui, Y. Electrospun Core-Shell Microfiber Separator with Thermal-Triggered Flame-Retardant Properties for Lithium-Ion Batteries. *Sci. Adv.* **2017**, *3* (1), No. e1601978.
(17) Li, Y.; Li, Y.; Pei, A.; Yan, K.; Sun, Y.; Wu, C.-L.; Joubert, L.-M.; Chin, R.; Koh, A. L.; Yu, Y.; et al. Atomic Structure of Sensitive Battery Materials and Interfaces Revealed by Cryo−Electron Microscopy. *Science* **2017**, *358* (6362), 506−510.
(18) Liu, N.; Zhou, G.; Yang, A.; Yu, X.; Shi, F.; Sun, J.; Zhang, J.; Liu, B.; Wu, C.-L.; Tao, X.; et al. Direct Electrochemical Generation of Supercooled Sulfur Microdroplets Well below Their Melting Temperature. *Proc. Natl. Acad. Sci. U. S. A.* **2019**, *116* (3), 765−770.
(19) Zheng, J.; Zhao, Q.; Tang, T.; Yin, J.; Quilty, C. D.; Renderos, G. D.; Liu, X.; Deng, Y.; Wang, L.; Bock, D. C.; et al. Reversible Epitaxial Electrodeposition of Metals in Battery Anodes. *Science* **2019**, *366* (6465), 645−648.
(20) Wu, Z.; Wang, H.; Xiong, P.; Li, G.; Qiu, T.; Gong, W.-B.; Zhao, F.; Li, C.; Li, Q.; Wang, G.; et al. Molecularly Thin Nitride Sheets Stabilized by Titanium Carbide as Efficient Bifunctional Electrocatalysts for Fiber-Shaped Rechargeable Zinc-Air Batteries. *Nano Lett.* **2020**, *20* (4), 2892−2898.
(21) Li, Y.; Dai, H. Recent Advances in Zinc-Air Batteries. *Chem. Soc. Rev.* **2014**, *43* (15), 5257−5275.
(22) Li, Y.; Lu, J. Metal−Air Batteries: Will They Be the Future Electrochemical Energy Storage Device of Choice? *ACS Energy Lett.* **2017**, *2* (6), 1370−1377.
(23) Wang, F.; Hu, E.; Sun, W.; Gao, T.; Ji, X.; Fan, X.; Han, F.; Yang, X.-Q.; Xu, K.; Wang, C. A Rechargeable Aqueous Zn^{2+}-Battery with High Power Density and a Long Cycle-Life. *Energy Environ. Sci.* **2018**, *11* (11), 3168−3175.
(24) Chen, C.-Y.; Matsumoto, K.; Kubota, K.; Hagiwara, R.; Xu, Q. A Room-Temperature Molten Hydrate Electrolyte for Rechargeable Zinc−Air Batteries. *Adv. Energy Mater.* **2019**, *9* (22), 1900196.
(25) Yi, J.; Liang, P.; Liu, X.; Wu, K.; Liu, Y.; Wang, Y.; Xia, Y.; Zhang, J. Challenges, Mitigation Strategies and Perspectives in Development of Zinc-Electrode Materials and Fabrication for Rechargeable Zinc-Air Batteries. *Energy Environ. Sci.* **2018**, *11* (11), 3075−3095.
(26) Li, Y.; Gong, M.; Liang, Y.; Feng, J.; Kim, J. E.; Wang, H.; Hong, G.; Zhang, B.; Dai, H. Advanced Zinc-Air Batteries Based on High-Performance Hybrid Electrocatalysts. *Nat. Commun.* **2013**, *4* (May), 1805−1807.
(27) Rojas-Carbonell, S.; Artyushkova, K.; Serov, A.; Santoro, C.; Matanovic, I.; Atanassov, P. Effect of PH on the Activity of Platinum Group Metal-Free Catalysts in Oxygen Reduction Reaction. *ACS Catal.* **2018**, *8* (4), 3041−3053.
(28) Zhang, J.; Zhou, Q.; Tang, Y.; Zhang, L.; Li, Y. Zinc−Air Batteries: Are They Ready for Prime Time? *Chem. Sci.* **2019**, *10* (39), 8924−8929.
(29) Bonnick, P.; Dahn, J. R. A Simple Coin Cell Design for Testing Rechargeable Zinc-Air or Alkaline Battery Systems. *J. Electrochem. Soc.* **2012**, *159* (7), A981−A989.
(30) Liu, J.; Guan, C.; Zhou, C.; Fan, Z.; Ke, Q.; Zhang, G.; Liu, C.; Wang, J. A Flexible Quasi-Solid-State Nickel−Zinc Battery with High Energy and Power Densities Based on 3D Electrode Design. *Adv. Mater.* **2016**, *28* (39), 8732−8739.
(31) Wang, L.; Yang, Z.; Chen, X.; Qin, H.; Yan, P. Formation of Porous ZnO Microspheres and Its Application as Anode Material with Superior Cycle Stability in Zinc-Nickel Secondary Batteries. *J. Power Sources* **2018**, *396* (April), 615−620.
(32) Yan, X.; Chen, Z.; Wang, Y.; Li, H.; Zhang, J. In-Situ Growth of ZnO Nanoplates on Graphene for the Application of High Rate Flexible Quasi-Solid-State Ni-Zn Secondary Battery. *J. Power Sources* **2018**, *407*, 137−146.
(33) Zhou, Z.; Zhang, Y.; Chen, P.; Wu, Y.; Yang, H.; Ding, H.; Zhang, Y.; Wang, Z.; Du, X.; Liu, N. Graphene Oxide-Modified Zinc Anode for Rechargeable Aqueous Batteries. *Chem. Eng. Sci.* **2019**, *194*, 142−147.
(34) Yan, Y.; Zhang, Y.; Wu, Y.; Wang, Z.; Mathur, A.; Yang, H.; Chen, P.; Nair, S.; Liu, N. A Lasagna-Inspired Nanoscale ZnO Anode Design for High-Energy Rechargeable Aqueous Batteries. *ACS Appl. Energy Mater.* **2018**, *1* (11), 6345−6351.
(35) Parker, J. F.; Chervin, C. N.; Pala, I. R.; Machler, M.; Burz, M. F.; Long, J. W.; Rolison, D. R. Rechargeable Nickel−3D Zinc Batteries: An Energy-Dense, Safer Alternative to Lithium-Ion. *Science* **2017**, *356* (6336), 415−418.
(36) Ko, J. S.; Geltmacher, A. B.; Hopkins, B. J.; Rolison, D. R.; Long, J. W.; Parker, J. F. Robust 3D Zn Sponges Enable High-Power, Energy-Dense Alkaline Batteries. *ACS Appl. Energy Mater.* **2019**, *2* (1), 212−216.
(37) Wu, Y.; Zhang, Y.; Ma, Y.; Howe, J. D.; Yang, H.; Chen, P.; Aluri, S.; Liu, N. Ion-Sieving Carbon Nanoshells for Deeply Rechargeable Zn-Based Aqueous Batteries. *Adv. Energy Mater.* **2018**, *8* (36), 1802470.
(38) Chen, P.; Wu, Y.; Zhang, Y.; Wu, T.-H.; Ma, Y.; Pelkowski, C.; Yang, H.; Zhang, Y.; Hu, X.; Liu, N. A Deeply Rechargeable Zinc Anode with Pomegranate-Inspired Nanostructure for High-Energy Aqueous Batteries. *J. Mater. Chem. A* **2018**, *6* (44), 21933−21940.
(39) Zhang, Y.; Wu, Y.; Ding, H.; Yan, Y.; Zhou, Z.; Ding, Y.; Liu, N. Sealing ZnO Nanorods for Deeply Rechargeable High-Energy Aqueous Battery Anodes. *Nano Energy* **2018**, *53*, 666−674.
(40) Lee, S.-M.; Kim, Y.-J.; Eom, S.-W.; Choi, N.-S.; Kim, K.-W.; Cho, S.-B. Improvement in Self-Discharge of Zn Anode by Applying Surface Modification for Zn−Air Batteries with High Energy Density. *J. Power Sources* **2013**, *227*, 177−184.
(41) Cho, Y.-D.; Fey, G. T.-K. Surface Treatment of Zinc Anodes to Improve Discharge Capacity and Suppress Hydrogen Gas Evolution. *J. Power Sources* **2008**, *184* (2), 610−616.
(42) Zhang, Z.; Yang, Z.; Huang, J.; Feng, Z.; Xie, X. Enhancement of Electrochemical Performance with Zn-Al-Bi Layered Hydrotalcites as Anode Material for Zn/Ni Secondary Battery. *Electrochim. Acta* **2015**, *155*, 61−68.
(43) Bian, S.-W.; Mudunkotuwa, I. A.; Rupasinghe, T.; Grassian, V. H. Aggregation and Dissolution of 4 nm ZnO Nanoparticles in Aqueous Environments: Influence of PH, Ionic Strength, Size, and Adsorption of Humic Acid. *Langmuir* **2011**, *27* (10), 6059−6068.
(44) Lee, S.; Yi, C.; Kim, K. Characteristics and Electrochemical Performance of the TiO_2-Coated ZnO Anode for Ni−Zn Secondary Batteries. *J. Phys. Chem. C* **2011**, *115* (5), 2572−2577.
(45) Laursen, A. B.; Varela, A. S.; Dionigi, F.; Fanchiu, H.; Miller, C.; Trinhammer, O. L.; Rossmeisl, J.; Dahl, S. Electrochemical Hydrogen Evolution: Sabatier's Principle and the Volcano Plot. *J. Chem. Educ.* **2012**, *89* (12), 1595−1599.
(46) Wang, J.; Zhong, H.; Wang, Z.; Meng, F.; Zhang, X. Integrated Three-Dimensional Carbon Paper/Carbon Tubes/Cobalt-Sulfide Sheets as an Efficient Electrode for Overall Water Splitting. *ACS Nano* **2016**, *10* (2), 2342−2348.

https://dx.doi.org/10.1021/acs.nanolett.0c01776
Nano Lett. 2020, 20, 4700−4707

(47) Xu, C.; Wu, J.; Desai, U. V.; Gao, D. High-Efficiency Solid-State Dye-Sensitized Solar Cells Based on TiO_2-Coated ZnO Nanowire Arrays. *Nano Lett.* **2012**, *12* (5), 2420−2424.
(48) Nai, J.; Yin, H.; You, T.; Zheng, L.; Zhang, J.; Wang, P.; Jin, Z.; Tian, Y.; Liu, J.; Tang, Z.; et al. Efficient Electrocatalytic Water Oxidation by Using Amorphous Ni−Co Double Hydroxides Nanocages. *Adv. Energy Mater.* **2015**, *5* (10), 1401880.
(49) Nørskov, J. K.; Bligaard, T.; Logadottir, A.; Kitchin, J. R.; Chen, J. G.; Pandelov, S.; Stimming, U. Trends in the Exchange Current for Hydrogen Evolution. *J. Electrochem. Soc.* **2005**, *152* (3), J23.
(50) Zheng, Y.; Jiao, Y.; Zhu, Y.; Li, L. H.; Han, Y.; Chen, Y.; Du, A.; Jaroniec, M.; Qiao, S. Z. Hydrogen Evolution by a Metal-Free Electrocatalyst. *Nat. Commun.* **2014**, *5*, 3783.
(51) Lim, M. B.; Lambert, T. N.; Ruiz, E. I. Effect of ZnO-Saturated Electrolyte on Rechargeable Alkaline Zinc Batteries at Increased Depth-of-Discharge. *J. Electrochem. Soc.* **2020**, *167* (6), 060508.
(52) Olivares-Ramírez, J. M.; Campos-Cornelio, M. L.; Uribe Godínez, J.; Borja-Arco, E.; Castellanos, R. H. Studies on the Hydrogen Evolution Reaction on Different Stainless Steels. *Int. J. Hydrogen Energy* **2007**, *32* (15), 3170−3173.
(53) Gao, Y.; Yan, Z.; Gray, J. L.; He, X.; Wang, D.; Chen, T.; Huang, Q.; Li, Y. C.; Wang, H.; Kim, S. H.; et al. Polymer−Inorganic Solid−Electrolyte Interphase for Stable Lithium Metal Batteries under Lean Electrolyte Conditions. *Nat. Mater.* **2019**, *18* (4), 384−389.
(54) Xue, W.; Shi, Z.; Suo, L.; Wang, C.; Wang, Z.; Wang, H.; So, K. P.; Maurano, A.; Yu, D.; Chen, Y.; et al. Intercalation-Conversion Hybrid Cathodes Enabling Li−S Full-Cell Architectures with Jointly Superior Gravimetric and Volumetric Energy Densities. *Nat. Energy* **2019**, *4* (5), 374−382.
(55) Pan, H.; Han, K. S.; Engelhard, M. H.; Cao, R.; Chen, J.; Zhang, J.-G.; Mueller, K. T.; Shao, Y.; Liu, J. Addressing Passivation in Lithium-Sulfur Battery Under Lean Electrolyte Condition. *Adv. Funct. Mater.* **2018**, *28* (38), 1707234.
(56) Turney, D. E.; Gallaway, J. W.; Yadav, G. G.; Ramirez, R.; Nyce, M.; Banerjee, S.; Chen-Wiegart, Y. K.; Wang, J.; D'Ambrose, M. J.; Kolhekar, S.; et al. Rechargeable Zinc Alkaline Anodes for Long-Cycle Energy Storage. *Chem. Mater.* **2017**, *29* (11), 4819−4832.
(57) Parker, J. F.; Ko, J. S.; Rolison, D. R.; Long, J. W. Translating Materials-Level Performance into Device-Relevant Metrics for Zinc-Based Batteries. *Joule* **2018**, *2* (12), 2519−2527.

https://dx.doi.org/10.1021/acs.nanolett.0c01776
Nano Lett. 2020, 20, 4700−4707